Application of optical diagnostics to the quantification of soot in n-alkane flames under diesel conditions

Authors:

José V. Pastor[1], José M. García-Oliver[1], Antonio García[1], Carlos Micó[1] and Sebastian Möller[2]

Affiliation:

1. CMT Motores Térmicos – Universitat Politècnica de València, Camino de Vera s/n, 46022, Valencia, Spain.
2. Kompetenzzentrum – Das Virtuelle Fahrzeug Forschungsgesellschaft mbH (ViF), Inffeldgasse 21/A/I, 8010, Graz, Austria.

Corresponding Author:

José V. Pastor

jpastor@cmt.upv.es

Tel. +34 963 879 654

Abstract

In the present paper, three different soot-measuring techniques, namely Laser Extinction Method (LEM), 2-Color Pyrometry (2C) and Laser-Induced Incandescence (LII) have been simultaneously employed to characterize soot distribution inside a diesel flame. Two single-component fuels (n-Decane and n-Hexadecane) and two derived blends (50%Dec/50%Hex and 30%Dec/70%Hex) have been used. Tests have been performed at an optical diesel engine, under different in-cylinder conditions. The study has been complemented with the measurement of ignition delay and Lift-off length.

The present work pursues a twofold objective. On the one hand, the effect of fuel properties on soot formation have been analysed, under different engine operating conditions. On the other hand, sensitivity and performance of the three optical techniques has been evaluated, identifying their main advantages and drawbacks in the framework of the current study. LEM has been considered as the reference technique, as the measurement principle can be implemented without important limitations associated to the other two. Results highlight that larger molecules produce more soot than the smaller ones, with both reactivity and soot formation changing with the proportion of the heavier fraction. Despite describing similar trends, LEM and 2C do not provide the same KL values, with the pyrometry reaching some sort of saturation when increasing flame soot. A detailed analysis confirms that 2-Color measurements are strongly biased by soot and temperature distribution inside the flame. Nevertheless, it could still be a good option for low sooting conditions. On the other hand, an attempt to calibrate LII signal by means of LEM measurements has been reported. This approach should make it possible to obtain additional information on the soot spatial distribution. However, inconsistencies have been identified which stem from the inherent limitations of LII technique in highly sooting conditions.

Keywords:

Soot Measurement, Laser induced incandescence, two-colour pyrometry, laser extinction method, n-alkane, Diesel combustion

1. INTRODUCTION

Optical diagnostic techniques have been traditionally used to improve the insight on the basic phenomena that dominate combustion within internal combustion engines. In particular, the characterization of the soot formation during combustion is a challenging topic, as it involves complex physical and chemical processes that dominate both formation and later oxidation [1, 2]. Three main optical techniques can be found in the literature for the study of this topic: Laser-Induced Incandescence (LII), 2-Colour Pyrometry (2C) and Laser Extinction Method (LEM). They have been applied traditionally to diesel flames, but they present certain advantages and drawbacks that must be considered before choosing the most suitable tool for each specific study.

LII is based on recording the high intensity radiation emitted by soot particles that are previously heated by a laser pulse. The magnitude of the signal can be correlated with the volume fraction of particles in the detection region. This technique has been used extensively for qualitative [3–6] and even quantitative measurements [7-9]. However, quantitative measurements require a firm understanding of the factors that influence the LII signal, which are detailed in [10]. As an intermediate step, calibration of LII signal with LEM measurements is quite often employed [11–16], in theory should make it possible to derive 2D soot volume fraction distributions. This approach, however, does not solve the inherent limitations of LII related to radiation attenuation processes within the flame.

2-Colour Pyrometry is based on the detection of the spontaneous thermal radiation emitted by incandescent soot particles at two different wavelengths. The technique makes it possible to obtain not only the soot distribution but also the corresponding temperature. Moreover, modern high-speed cameras offer a high time resolution. This technique has been widely used by the diesel engine research community [17-27]. However, the analysis of results does not always consider the intrinsic limitations of the technique [22, 23].

While 2C and LII could be strongly affected by the interaction of emitted radiation with other soot particles within the flame, the third technique, LEM, is just based on this property. The attenuation can be related to the optical thickness of the soot cloud and, eventually, to the soot volume fraction. This technique has been widely used in single diffusion flames [28-31] and, with the proper considerations [30], reliable results can be obtained. LEM applications are based on point measurements along the flame, using a small laser beam. It allows high time resolution but it is spatially limited by the beam size. However, nowadays applications start to appear where a larger light source is combined with high-speed cameras, offering both good spatial and time resolution [32].

In the present work, the three techniques (LII, 2C and LEM) have been proposed to characterize soot formation under diesel engine conditions. They have been applied simultaneously, to evaluate the effect of physical and chemical properties of two single-component surrogates (n-Decane and n-Hexadecane) and two derived blends. The analysis of experimental results will make it possible to fulfil a twofold objective: firstly, describe the effect of fuel properties over soot formation; secondly, identify the strengths and limitations of each methodology. The first part of the paper presents a detailed description of the experimental apparatus and procedure. Then, a comparison among results obtained by each technique is presented. Trends and numerical results are analysed and discussed, trying to clarify the main differences observed. Finally, the main conclusions regarding the influence of fuel properties and the optical techniques, together with recommendations for the proper use of these experimental tools, will be summarized.

2. EXPERIMENTAL METHODOLOGY

2.1. Experimental Test Bench

All the tests have been performed at an optically accessible single cylinder engine, which is described in detail in [33]. The facility is based on a 2-stroke single cylinder direct injection diesel engine (Jenbach JW 50), with three liter displacement and 15.7 effective compression ratio. It is motored at low engine speed (500 rpm). Intake and exhaust processes are handled by transfers on the liner and the cylinder head is specially designed to provide optical access to the combustion chamber. A cylindrical combustion chamber was designed in a way that spray wall impingement is avoided. The chamber has an upper port where the injector can be mounted and four lateral accesses. A pressure transducer is installed in one of the accesses, whereas the other three are equipped with oval-shaped quartz windows, 88 mm long, 37 mm large and 28 mm thick. A cutaway view of the cylinder head is depicted in Figure 1. The cylinder head and the engine temperature are controlled by means of coolant recirculation. Their temperature was set to 353 K, to guarantee a good performance of the lubricant oil.

In-cylinder thermodynamic conditions during the cycle are controlled by the intake air temperature and pressure. The first one is regulated by two sets of electrical resistors, while the desired intake pressure is achieved thanks to a compressor that is fed with ambient air. The engine is operated under skip-fired mode, so that in-cylinder conditions are not influenced by the remaining residual gases from previous combustion cycles. An injection takes place each 30 cycles, which guarantees that ambient conditions are kept constant between consecutive repetitions and temperature transients are avoided.

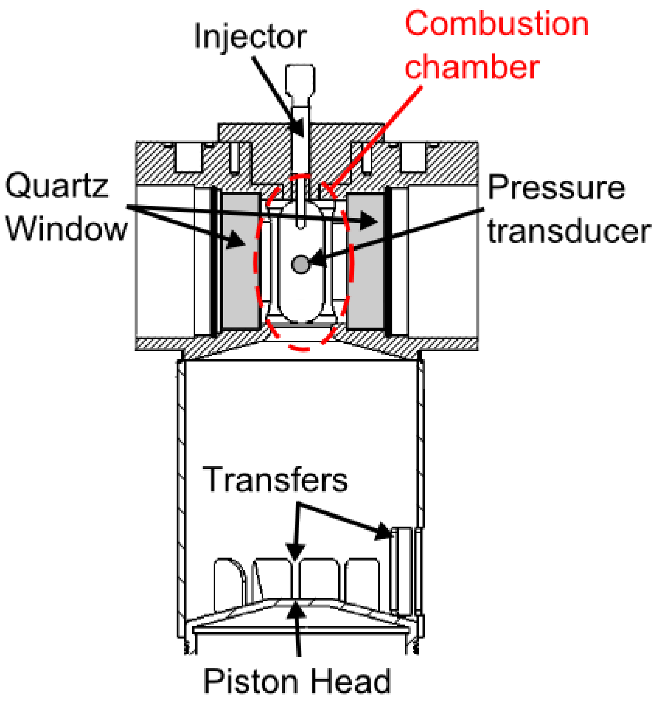

Figure 1 Cutaway view of the cylinder head layout

A common-rail injection system is used, together with a single-hole piezoelectric injector with a 140 μm outlet diameter nozzle. The injector hole is 1 mm long with conical shape (Ks factor of 1.5). The injected mass is so low that thermodynamic conditions inside the combustion chamber are barely affected by the fuel evaporation [24]. Due to the low injection frequency used during tests, the injected fuel initial temperature can be considered the same.

2.2. Experimental procedure

Two single-component fuels have been used, namely n-Decane and n-Hexadecane, together with two derived binary blends: 50%Decane/50%Hexadecane and 30%Decane/70%Hexadecane (percentages in mass). The main advantage of using such simple fuels is that it is expected that they will form less soot than other fuels like commercial diesel, thanks to the absence of ring or branched structures as well as sulphur [2]. The most relevant properties of the fuels for the purposes of this work are given in *Table 1*.

Fuel	Density at 373 K [Kg/m^3]	Formula	Derived Cetane number	C-C Bonds	H/C
n-Decane	669.2	$C_{10}H_{22}$	65.9	9	2.19
50Dec/50Hex	693.9	-	82.2	11.37	2.16
30Dec/70Hex	703.7	-	85.4	12.56	2.14
n-Hexadecane	718.5	$C_{16}H_{34}$	92.9	15	2.12

Table 1 Fuel properties.

The full test matrix comprises a combination of two in-cylinder top dead center (TDC) temperature values (800/900 K) with three different TDC pressure values (4.3, 5.3 and 7.3 MPa) and three injection pressures (50/100/150 MPa). In-cylinder thermodynamic conditions (Figure 2 -right-) have been calculated from measured in-cylinder pressure, using a first-law thermodynamic analysis as it can be found in [31, 33]. The model takes into account blow-by, heat losses and mechanical deformations. The trapped mass is estimated using the intake temperature and volume at the exhaust vent close. Then, temperature along the engine cycle can be calculated using the equation of state and correcting the trapped mass with blow-by estimations.

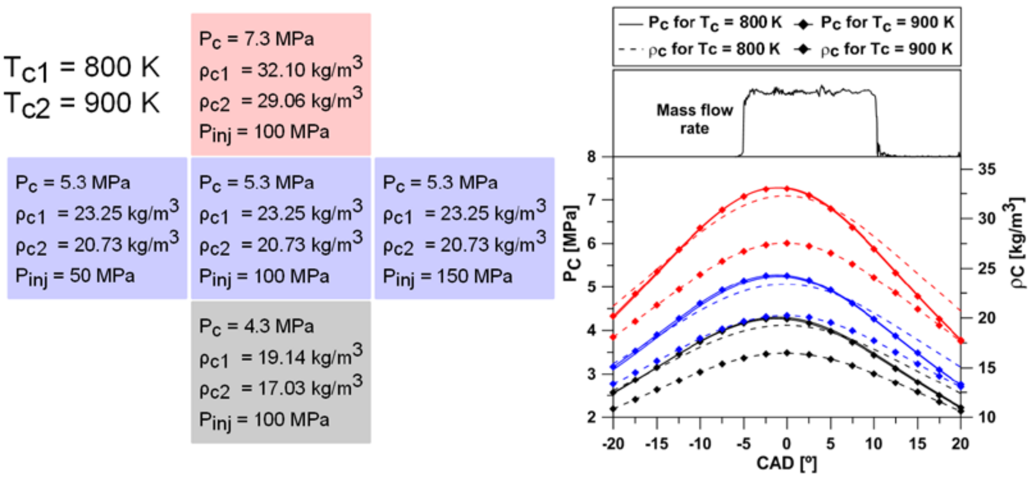

Figure 2 Test matrix (left) and the corresponding thermodynamic conditions in the combustion chamber

As previously mentioned, three different optical techniques have been applied simultaneously to measure soot formation inside the flame. The injector energizing time was set to 3 ms (9 CAD) for all conditions, which results in an approximate 6 ms (18 CAD) real injection duration, considering electrical and hydraulic delays. The injector was triggered at 6 CAD before TDC (SoE), while the injection started at approximately 5 CAD before TDC (SoI), so that the variations of the in-cylinder thermodynamic conditions during the injection event were minimized. The 2-Color Pyrometry and Laser Extinction Method are able to measure the soot formation during the whole combustion event, thanks to the high sampling rate of the detectors. On the one hand, two high-speed cameras (2C) were set to start registering the light emitted by the flame at SoE, with $\Delta t = 66\ \mu s$ (0.2 CAD) between two consecutive frames. On the other hand, a fast-response photodiode (LEM) was continuously measuring the intensity of a laser that was aligned perpendicular to, and intersecting, the flame axis. Finally, for each injection event a Nd:YAG laser was fired at 3 CAD after SoE, to measure the induced incandescence from soot. This instant was chosen in order to guarantee the stabilization of the diffusion flame before the laser was fired.

2.3. Optical System

Different optical techniques have been applied simultaneously, taking advantage of the three available optical accesses located in the cylinder head. The optical arrangement is shown in Figure 3. In the following subsections, a more detailed description on the soot techniques is presented. Additionally, images of OH* radiation with an ICCD camera were recorded simultaneously with the soot measurements. The procedure and results are summarized in Appendix 1.

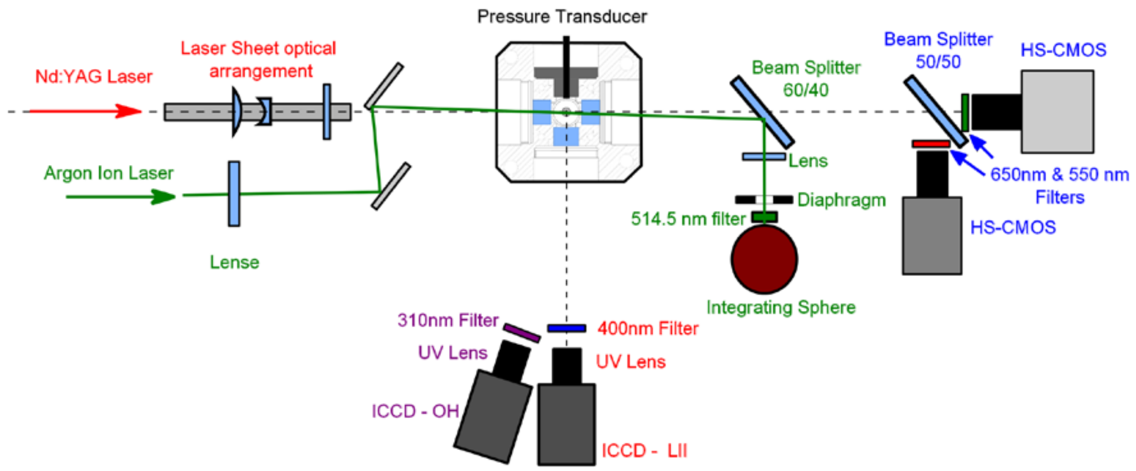

Figure 3 Schematic of the optical arrangement.

2.3.1. Laser Extinction Method

The Laser Extinction Method is based on the attenuation that a light beam undergoes when it traverses a soot cloud, which is quantified in terms of the Lambert-Beer's law as:

$$I = I_0 exp(-K_{LEM} L) \quad (1)$$

where I and I_0 are the attenuated and original intensities, K_{LEM} is the dimensional extinction coefficient of the cloud of particles and L is the path length, which corresponds to the size of the cloud in the direction of the light beam. The extinction coefficient can be expressed as:

$$K_{LEM} = \frac{k_{soot} f_v}{\lambda} \qquad (2)$$

where f_v is the soot volume fraction, λ is the laser wavelength and k_{soot} is the dimensionless extinction coefficient. The optical arrangement set for the Laser Extinction Method is shown in Figure 3. A continuous Argon laser was set to cross the combustion chamber through two aligned optical accesses. The laser was tuned at 514.5 nm with 400 mW and oriented with a 1 degree angle of incidence in relation to the entrance quartz window due to space and optics limitations. Besides, it was observed that this orientation made it possible to remove any influence of the etalon effect on the measurements [30]. In order to minimize the divergence of the laser, a 500 mm focal length lens was set just at the output of the fiber optics that were used to guide the beam from the laser output towards the test rig. The minimum beam waist (300 μm diameter) was located in the region of the flame and the laser beam was aligned in a way that it was crossing the flame axis. Once the laser left the combustion chamber, it was reflected by a beam splitter (60% Transmission – 40% Reflection) towards the collection optics. .

Musculus et al. [30] present an extended analysis of several uncertainty sources that must be considered when LEM is applied. Two major issues were identified: beam steering and the contamination of measurement by light coming from the flame. The first one is a consequence of the refractive index gradients inside the combustion chamber due to fuel evaporation and combustion. In order to minimize this effect, a 50 mm diameter lens was placed just after the beam splitter, to collect deviated rays up to a maximum divergence angle of 150 mrad. If the maximum divergence angle collected is too large, the light emitted by the flame can be also registered leading to an underestimation of the light extinction. In this sense, a diaphragm was located at the focal plane of the lens to limit the maximum divergence angle to 100 mrad [30]. Finally a bandpass filter was placed between the diaphragm and the detector (centered at 514 nm with 10 nm FWHM) to reject the major part of the flame radiation. The detector is a fast response photodiode, connected directly to an integrating sphere.

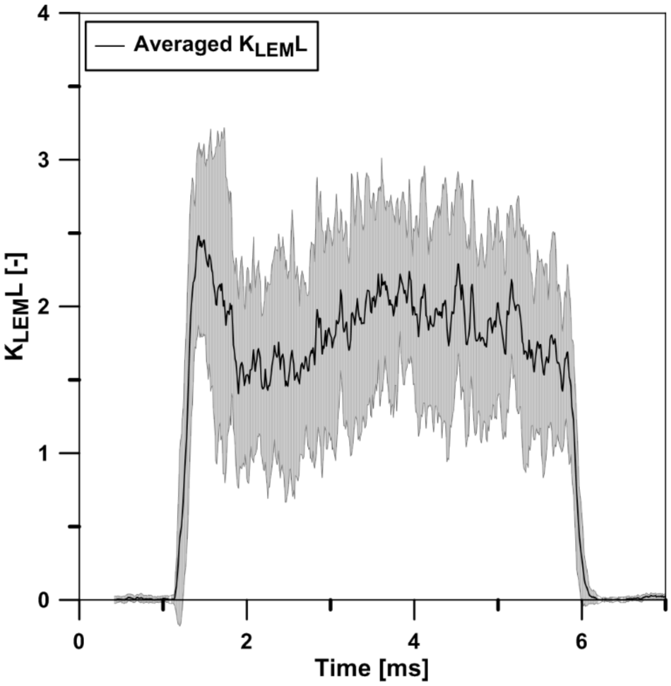

Figure 4 Average $K_{LEM}L$ and standard deviation for P_c = 5.3 MPa, T_c = 900 K and P_{inj} = 100 MPa, at 50 mm from nozzle tip.

Light extinction was measured at several positions along the spray axis: 33 mm, 42 mm, 51 mm and 60 mm for two nominal conditions (P_c = 5.3 MPa, P_{inj}= 100 MPa and the two in-cylinder temperatures), and only at 33 mm and 51 mm for the rest of conditions. In order to calculate the instantaneous transmissivity of the flame, the attenuated intensity from each combustion event is compared with the intensity registered in the previous motored cycle (equation -1-). This ensures that effects like window fouling or intensity variations from the laser do not affect measurements. In Figure 4, an example of $K_{LEM}L$ evolution is presented. The black line shows the $K_{LEM}L$ averaged between 15 repetitions. The grey area represents is limited by ± one standard deviation, which is not negligible. A similar behaviour was previously reported by Payri et al. [31], where the authors analyse the scattering inherent to the test rig.

2.3.2. 2-Color Pyrometry

2-Color Pyrometry is based upon recording of spontaneous soot incandescence. The intensity of such radiation source (I_{soot}) is equal to the product of the radiation emitted by a black body at the same temperature (T) and the emissivity of the particles, which can be expressed in terms of soot concentration, working wavelength (λ) and a dispersion exponent (α) [22]. Therefore, I_{soot} can be expressed as the following equation:

$$I_{soot}\,(\lambda, T, KL) = \left[1 - exp\left(-\frac{K_{2C}L}{\lambda^{\alpha}}\right)\right]\frac{1}{\lambda^5}\frac{c_1}{\left[exp\left(\frac{c_2}{\lambda T}\right)-1\right]} \qquad (3)$$

where c_1 = 1.1910439 x 10^{-16} Wm^2sr^{-1} and c_2 = 1.4388 x 10^{-2}mK. Zhao et al. [19] reported that α is less dependent on the wavelength in the visible range than in the infrared. According to that, 550 and 650 nm have been chosen for this work, so that α = 1.39 for most of the fuels [34]. The dependence of the emissivity on the soot amount within the optical path is usually expressed in terms of $K_{2C}L$. This variable accounts for the total contribution of the soot along the optical path, no matter either the soot distribution or geometrical size.

Two CMOS sensors were employed to measure soot radiation. The signal recorded signal S_λ can be expressed after several simplifications can be applied [22] according to equation (4):

$$S_\lambda = C_\lambda I_{soot}(\lambda, T, KL) \qquad (4)$$

where C_λ is a constant that quantifies the effects of the area A of the sooting flame within the field of view of the detector, the solid angle Ω and the wavelength λ. The two first parameters being constant, C_λ is calculated by means of a radiance calibration procedure as described by Payri et al. [22].

In the setup shown in Figure 3, light emitted by the sooting flame crossed a first beam splitter (60% transmission – 40% reflection), which was placed to reflect the LEM laser. Then, a second beam splitter is used to transmit and reflect 50% of the soot radiation to each of the two high-speed CMOS cameras employed (Phantom V12 for 650 nm, and Photron SA5 for 550 nm). Both cameras were equipped with a 100 mm focal length and f/2 lens and an interference filter, centred at 650 nm and 550 nm respectively with 10nm FWHM. Images were recorded at 15000 fps, with 5 to 8 us exposure time for 650 nm and 8 to 12 us for the 550 nm, depending on test conditions. To match both images on a pixel by pixel basis, a spatial transformation matrix is calculated, considering translation, rotation and scaling. For both images, background segmentation is also applied. A threshold value is obtained, considering a percentage of the total dynamic range of each image. The value of this percentage was set to 5% for all the tests, which has shown a good accuracy on the flame boundary detection for all the tests.

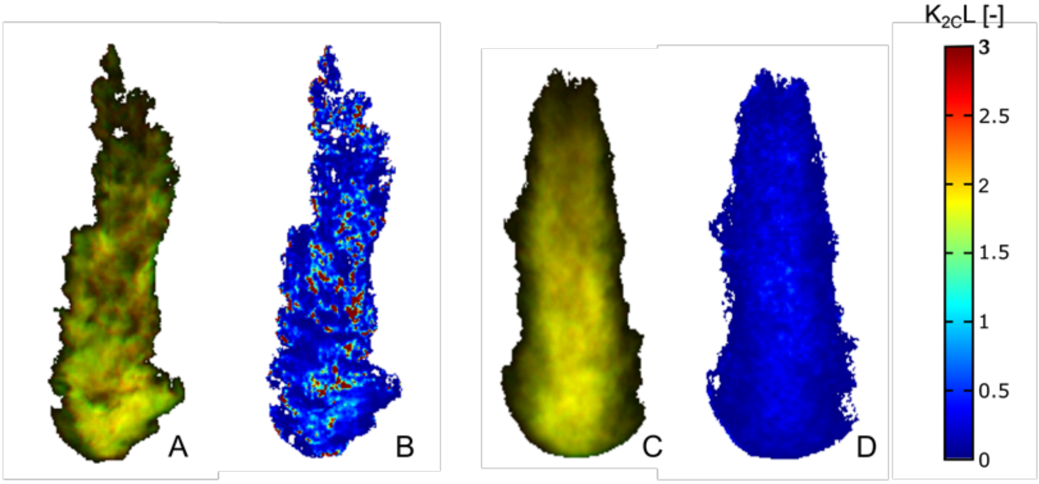

Figure 5 Composition of instantaneous (A) and average (C) soot natural luminosity at 550 and 650 nm and the corresponding $K_{2C}L$ (B and D) distributions. Data were taken for n-Decane, at P_c = 5.3 MPa, T_c = 900 K and P_{inj} = 100 MPa.

Once both images are coupled, equation (3) is applied for each wavelength and $K_{2C}L$ and temperature can be obtained. In Figure 5, an example of the application is shown. A colour composition of the instantaneous soot natural luminosity for 550 nm and 650 nm (A) is presented, together with the calculated map of $K_{2C}L$ (B). It is possible to see that the $K_{2C}L$ distribution is not homogeneous and even some spots of constant $K_{2C}L$ = 3 are observed. These spots are artificially introduced, and are formed by pixels where the combination of radiation at the two wavelengths leads to a non-physical solution. In Figure 6, radiance values at 550 and 650 nm for each pixel of the flame shown in Figure 5 are presented. Moreover, three curves are plotted which represent the different combinations of radiation that lead to $K_{2C}L$ = 0.1 (green), $K_{2C}L$ = 0.5 (blue) and $K_{2C}L$ = 3 (red). When $K_{2C}L$ increases, its emissivity tends asymptotically to 1 (black body). For $K_{2C}L$ = 3, the corresponding emissivity at 550 nm is 0.999. Therefore, the red curve can be interpreted as a frontier of the 2C methodology. Different uncertainty sources [21, 22] can lead to a combination of intensities of radiation located in the red area of Figure 6, which leads to a non-physical solution. When this happens, it is not possible to obtain a value of $K_{2C}L$ for such pixels and maximum $K_{2C}L$ = 3 is assigned. A similar heterogeneous distribution was previously reported by other authors [21, 26, 27]. Svensson et al. [21] suggest that the heterogeneity is real and not caused by uncertainty sources. However, Payri et al. [22] conclude that their influence is not negligible, leading to variations of $K_{2C}L$ up to 20%. To minimize the effect of such non-physical pixels, the 2C method is applied to the ensemble-averaged imaged at each time position (Figure 5 - C), similar to Yan et al. [17]. Corresponding $K_{2C}L$ results are presented in Figure 5 - D. In that way, the influence of measurement uncertainties such as read noise are minimized. The KL distribution shown in Figure 5 – D also shows that the number of pixels with non-physical solutions are reduced.

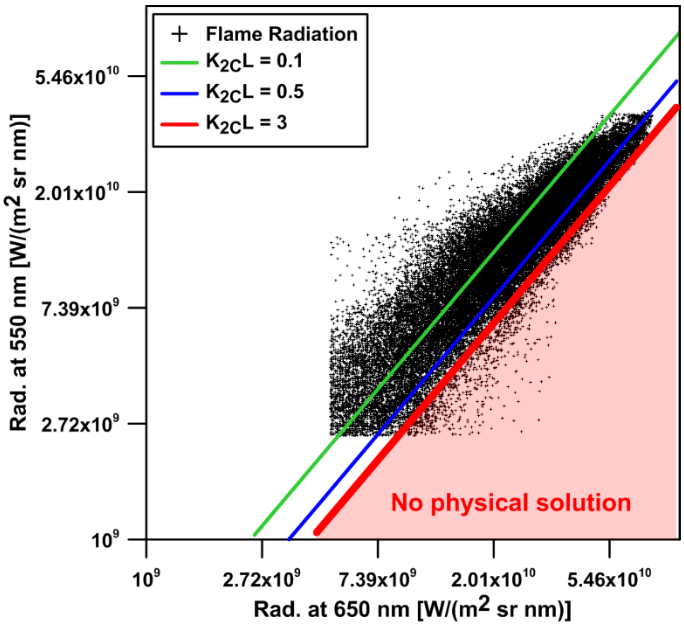

Figure 6 Intensity of radiation for each pixel of a flame, at 550 and 650 nm. Data was taken for n-Decane, at P_c = 5.3 MPa, T_c = 900 K and P_{inj} = 100 MPa.

2.3.3. Laser-Induced Incandescence

Laser-Induced Incandescence is based on the thermal radiation emitted by a soot cloud, when it is irradiated with an intense laser pulse that increases its temperature, with a corresponding increase in local radiation. In the present contribution, a laser sheet was created to heat the soot particles at the symmetry plane of the flame. A Nd:YAG laser pulse at 1064 nm was used, with 600 mJ/pulse and a Gaussian intensity profile. The main wavelength of this laser was chosen to avoid the PAH fluorescence, as it has been previously reported by Bobba et al. [4]. Three cylindrical lenses were used to obtain a 45 x 0.35 mm^2 collimated laser sheet, with 450 mJ/pulse at the entrance of the combustion chamber. The equivalent energy fluence is 2.87 J/cm^2, which is large enough to get a signal independent of the laser pulse energy as it has been previously reported by other authors [4, 13, 16]. However, care must be taken during analysis as this high energy fluence could evaporate the smallest soot particles. The laser sheet was located to obtain LII signal from 22 to 67 mm from the injector nozzle, covering a similar range as the LEM measurement. The signal was registered by a 16-bit intensified CCD camera (LaVision Dynamight), equipped with a 100 mm focal length and f/2 UV lens. A low pass filter with the cutting wavelength at 400 nm was placed in front of the detector, to improve the separation between LII and natural luminosity from the flame. Nevertheless, for each test, five background radiation images were recorded, ensemble-averaged and substracted from the LII signal. Such background levels were around 10% of the LII signal. It must be noted that this procedure is not an instantaneous correction. Therefore, it can be introducing local errors when single repetitions are considered. A 50 ns gate width was chosen, to minimize the influence of ambient conditions and possible electronic jitter between the laser and the camera [13].

2.4. Evaluation strategy for soot quantification techniques

One of the main goals of the present contribution is a comparison among all three diagnostic techniques. For that purpose, KL values (optical thickness) have been chosen as metrics of soot measurements [6, 30, 31, 35]. In this sense, a discussion regarding soot optical properties is avoided. According to the literature survey, LEM measurements have been chosen as reference, so performance and limitations of 2C-Pyrometry and LII can be analysed relative to this technique.

Under the assumption of thermal equilibrium, the emissivity of the soot cloud equals its absorptivity (Kirchhoff's law). Moreover, if the interaction between light and soot particles is in the Rayleigh regime, absorption would be dominant and scattering could be disregarded. Therefore, the emissivity of the 2-Color Pyrometry and LEM absorption can be compared as follows:

$$1 - \exp(-K_{LEM}L) = 1 - exp\left(\frac{-K_{2C}L}{\lambda^{\alpha}}\right) \qquad (5)$$

where $K_{LEM}L$ is the optical thickness obtained by means of LEM. To compare both techniques, the same physical magnitude has to be used. At this point, nomenclature in the literature is inconsistent, as both extinction and 2C derived results are defined as KL. Therefore, $K_{2C}^{*} = K_{2C}/\lambda^{\alpha}$ has been defined, which should enable a direct comparison between 2C and LEM, i.e. $K_{2C}^{*} = K_{LEM}$. Hence, considering that the wavelength used for laser extinction was 514.5 nm and α = 1.39, the following relationship can be derived in this case:

$$K_{LEM}L = K_{2C}^{*}L = 2.519 \cdot K_{2C}L \qquad (6)$$

which allows comparing the optical thickness of the flame obtained by means of LEM with 2C measurements. Note that the right-hand side of equation (5) is a semi-empirical derivation where λ is to be expressed in µm.

On the other hand, the starting point of LII technique is the assumption that the recorded signal is proportional to the soot volume fraction [19], equation (7):

$$f_v = C \cdot I_{LII} \qquad (7)$$

where f_v is the soot volume fraction, C is a constant and I_{LII} is the registered LII signal intensity at each pixel. The calculation of C can be addressed in two different ways. The first one is based on numerical approaches to characterize all the physical phenomena involved in the process. Different theoretical models can be found in the literature [10]. However, all of them show high complexity, especially under engine conditions. The second procedure is based on an empirical calibration by means of an additional experimental technique [11-16]. Despite certain limitations, results suggest that at least some semi-quantitative results on the soot distribution can be obtained. Following this approach, if equation (2) and (7) are combined, the following expression can be obtained:

$$K_{LEM} = C\frac{k_{soot}}{\lambda} \cdot I_{LII} = \frac{1}{C^*} \cdot I_{LII} \qquad (8)$$

As the comparison between LII and LEM has to be done in integrated values along the optical path, an integrated LII signal S_{LII} is defined as:

$$S_{LII} = \int_0^L I_{LII} dx \qquad (9)$$

and by integration of equation (8) the following expression is obtained:

$$S_{LII} = C^* K_{LEM} L \qquad (10)$$

As previously discussed, the calibration constant C* has been calculated by comparing $K_{LEM}L$ measurements with the corresponding I_{LII} integrated along the optical path (the width of the flame). Once the calibration constant is obtained, a LII-derived optical thickness for λ = 514.5 nm has been calculated ($K_{LII}L$) to enable a comparison with LEM and 2C results according to equation (11).

$$K_{LII} L = \frac{1}{C^*} S_{LII} \qquad (11)$$

In Figure 7, the comparison between S_{LII} and $K_{LEM}L$ for n-Decane is shown. 360 different measurement points are plotted which include all the different test conditions and the LEM measurement positions. $K_{LEM}L$ values correspond to the average of the last 50 µs just before the LII laser is fired, to minimize scattering caused by the measuring technique (Figure 4).

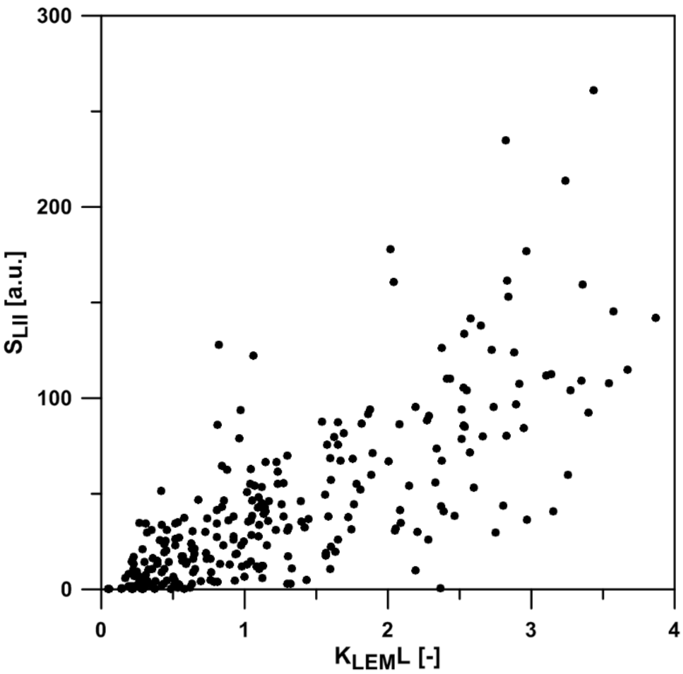

Figure 7 Correlation between $K_{LEM}L$ and S_{LII} for n-Decane. Single shot values.

Even though this issue was left aside in the previous theoretical derivation, attenuation of laser sheet along the soot cloud as well as subsequent signal trapping of emitted LII signal limit the applicability of LII for soot quantification. Such effects are present in Figure 9, from which the existence of a linear relationship between $K_{LEM}L$ and S_{LII} seems to be doubtful. De Francqueville et al. [13] suggested that one of the main uncertainty sources was the signal trapping effect. Cenker et al. [16] observed a similar scattering but, in this case, signal trapping was discarded and it was attributed to a combination of different uncertainty sources from both techniques.

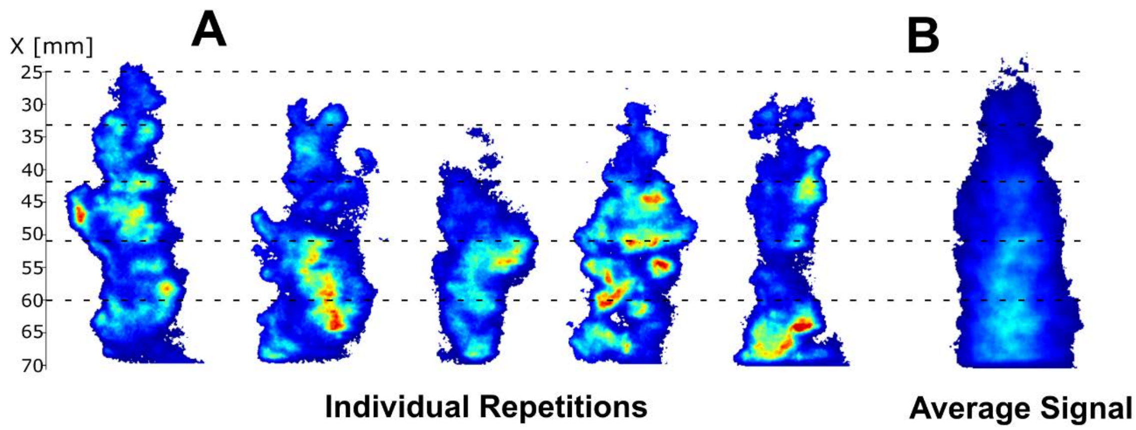

Figure 8 Comparison between individual repetitions and the averaged signal for n-Decane, at P_c = 5.3 MPa, T_c = 900 K and P_{inj} = 100 MPa. The dashed lines represent the positions where laser extinction was measured.

In Figure 8 (A), single-shot LII images for different n-Decane injections are shown. Scattering is clearly present among different repetitions and, what is more, the flame is not perfectly axisymmetric. The authors consider that this behaviour is inherent to the operating conditions of the test rig, caused by the interaction between the spray and the air flow inside the combustion chamber, which was previously analysed by Payri et al. [31]. In that work a strong scattering observed on LoL and $K_{LEM}L$ measurements was also reported. However, if the ensemble-averaged LII signal is observed (Figure 8 -B-), the assumption of axisymmetry still seems to be reasonable. Following this approach, Figure 9 shows the same relationship as Figure 7 based on ensemble-averaged values (sample size 75 repetitions for nominal points, i.e. P_c = 5.3 MPa and P_{inj} = 100 MPa, and 30 for other conditions). Data from all fuels have been included. Based on a linear regression (R^2 = 0.942) the calibration constant C* for the whole data set can be obtained, which is independent of fuel and in-cylinder conditions.

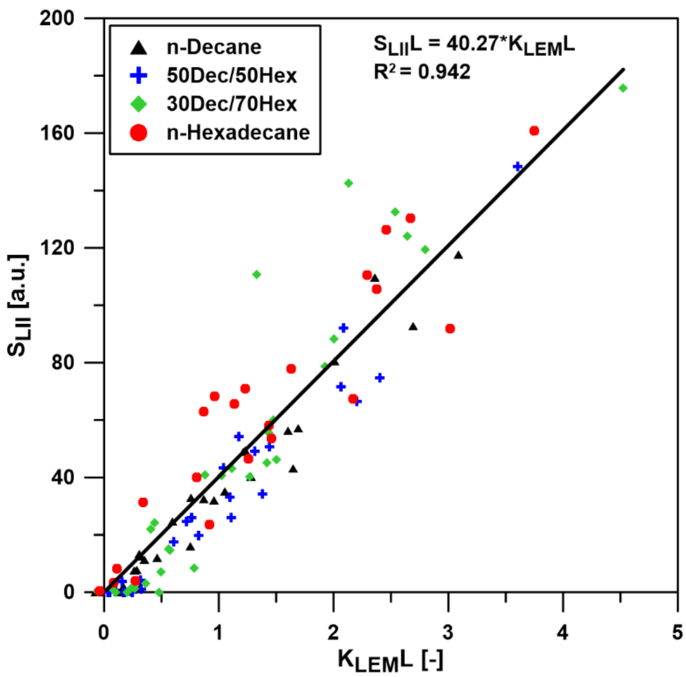

Figure 9 Comparison between $K_{LEM}L$ and S_{LII} for the four fuels. Ensemble-averaged values.

Summing up, individual cycle realization show hardly any correlation between the LEM and LII signals, but when using ensemble-averaged ones the situation improves. Based upon previous experiences with this experimental setup [31], where a strong cycle-to-cycle is present, coupled to the 1º inclination angle between the LEM point laser and the LII laser sheet could be a strong reason why a single realization comparison may not be fully correlated. When using ensemble-averaged values, the assumption of axissymmetry is recovered, and the correlation between both signals improves. However, some scattering is still present, which hints at the presence of absorption phenomena. Therefore LII results should be used in a semi-quantitative way. More discussion on such effects will be shown in Section 4.

3. FUEL EFFECTS ON SOOT DISTRIBUTION

LEM, 2C and LII have been utilized to study the effect of fuel properties over soot formation. However, a direct comparison between the different techniques also makes it possible to determine reliability and limitations of each of them. As previously mentioned, LEM has been chosen as reference and is compared with 2C and then LII. From Figure 10 to Figure 12, KL measurements on the flame axis are presented for the four fuels at three different ambient conditions, which have been selected from the test matrix as representative of low (Pc= 4.3 MPa, Tc= 800K), medium (Pc= 5.3 MPa, Tc= 800K) and high (Pc= 5.3 MPa, Tc= 900K) sooting conditions. $K_{LEM}L$ values correspond to the average of the last 50 µs just before the LII laser is fired. $K_{2C}^{*}L$ values correspond to the 2C results obtained at 3 CAD after TDC, coinciding with the LII measurement. For each LEM position, 15 LII images were recorded, which means that the LII signal is averaged from 75 different images for the nominal points (P_c = 5.3 MPa and P_{inj} = 100 MPa) and 30 for the rest of the tests matrix. $K_{LII}L$ is derived by means of equation (11).

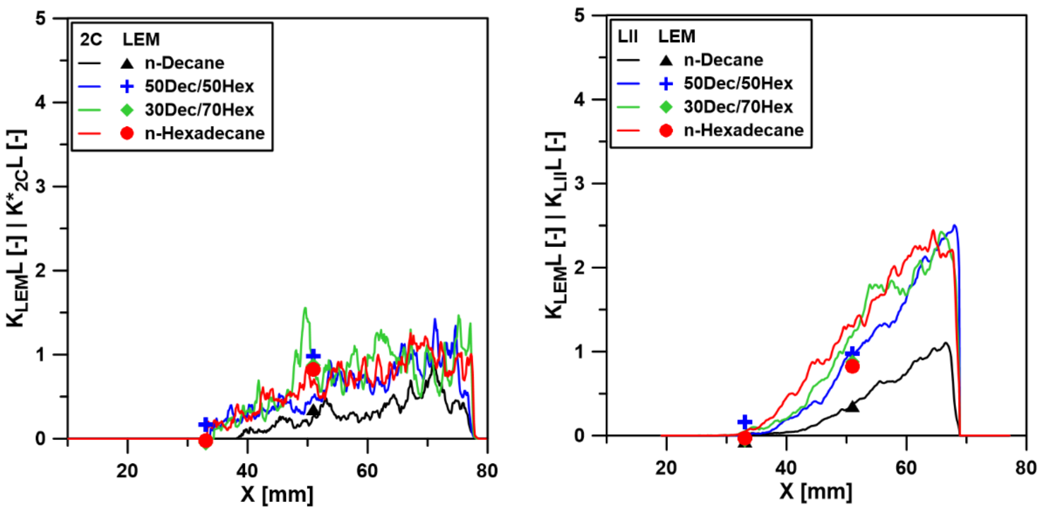

Figure 10 $K_{LEM}L$, $K_{2C}^{*}L$ (left) and $K_{LII}L$ (right) on the flame axis, for the four fuels at 800 K in-cylinder temperature, P_c = 4.3 MPa and P_{inj} = 100 MPa.

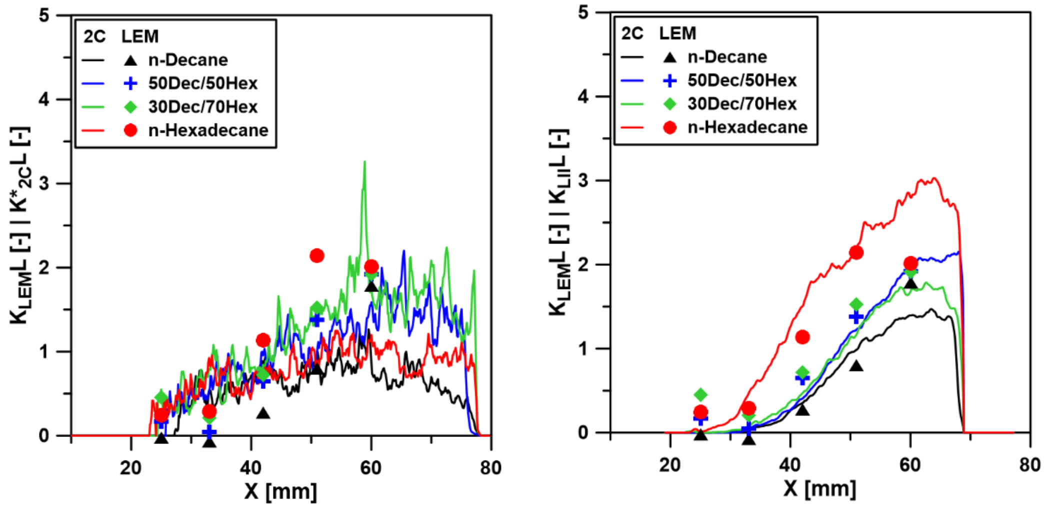

Figure 11 $K_{LEM}L$, $K_{2C}^{*}L$ (left) and $K_{LII}L$ (right) on the flame axis, for the four fuels at 800 K in-cylinder temperature, P_c = 5.3 MPa and P_{inj} = 100 MPa.

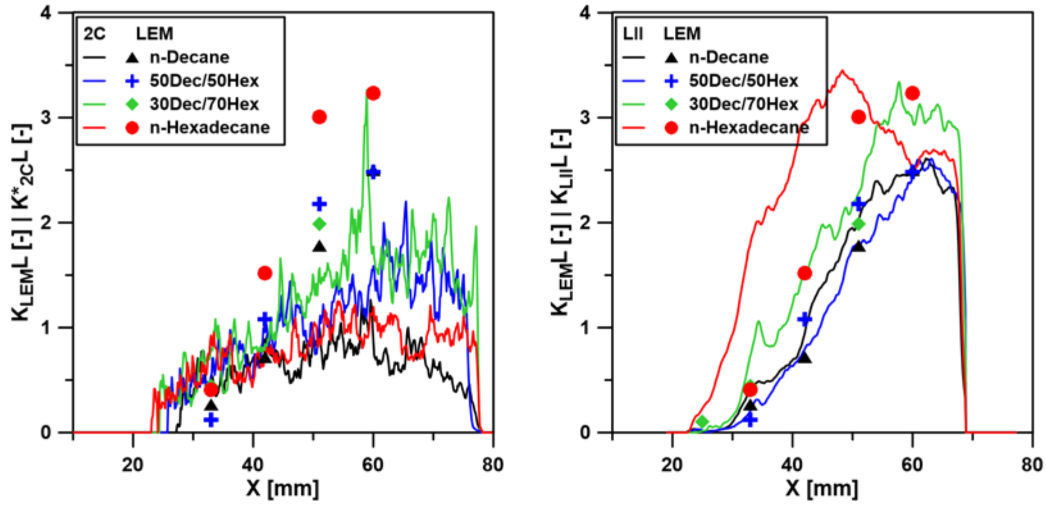

Figure 12 $K_{LEM}L$, $K_{2C}^{*}L$ (left) and $K_{LII}L$ (right) on the flame axis, for the four fuels at 900 K in-cylinder temperature, P_c = 5.3 MPa and P_{inj} = 100 MPa.

If LEM is used as a reference, soot is observed to effectively increase with ambient density. Such a result is consistent with literature studies [29, 31], and can be justified based on the reduction in lift-off length (LoL) that occurs with ambient density, which increases the equivalence ratio at the flame base, and hence induces higher soot formation. LoL values derived from OH* chemiluminiscence images recorded simultaneously with the soot measurements (Appendix 1) confirm such a reduction for the present test matrix.

On the other hand, for a given operating condition LEM measurements evidence that the increase in n-Hexadecane content results in more soot being formed. Two main factors contribute to such a trend. On the one hand, simultaneous OH* measurements for this fuel sweep (Figure 17) indicate that LoL is reduced with the increase of n-Hexadecane, due to the increased reactivity of this fuel (higher CN). As the mixing field is quite similar for all investigated fuels, this results in an increase of the equivalence ratio at the flame base, which enhances soot formation. On the other hand, the Threshold Sooting Index (TSI) is also observed to increase when shifting to larger alcanes [37], which means that the fuel is more prone to form soot.

A summary of the aforementioned trends with fuel composition is presented in Figure 13. $K_{LEM}L$ for n-Decane is compared with the other three fuels for all investigated conditions. Although some scattering is present, such a plot confirms the observed result in Figures 10 to 12.

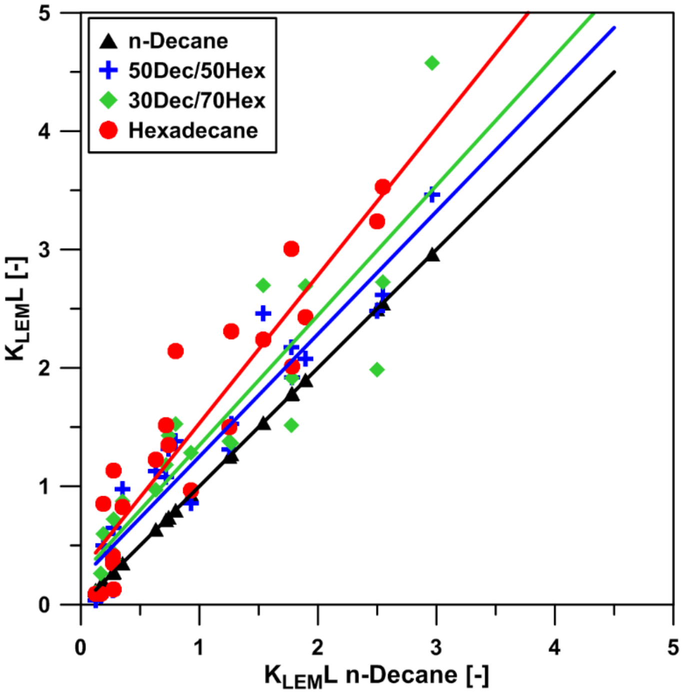

Figure 13 Comparison between $K_{LEM}L$ of n-Decane and the other three fuels.

4. DISCUSION ON SOOT DIAGNOSTICS

The previous section has shown the spatially resolved results obtained for the investigated conditions and fuels keeping LEM as the reference technique. This section will provide further discussion on the other two optical techniques.

On the one hand, 2C is observed to be quite insensitive to operating conditions, especially when shifting from medium to high density conditions (Figures 11 and 12). Even for a single operating condition, the increase of $K^*_{2C}L$ along the spray axis is quite modest in comparison with $K_{LEM}L$ evolution. In terms of fuel, only decane is consistently in the low range of measured values, while the trends among the other fuels are difficult to discern. Both statements confirm that, if any sensitivity in 2C is to be obtained, it mainly occurs in the low soot range. Figure 14 summarizes these findings on a one-to-one comparison between techniques. In general, it can be stated that values provided by 2C are lower than the ones obtained by LEM. Furthermore, these differences are shown to increase when the optical thickness of the flame increases (larger $K_{LEM}L$). Svensson [38] also reported differences in experimental optical thickness from the two techniques, with maximum values between 4.49 and 2.66 for $K_{LEM}L$, and between 1.3 and 1.02 for $K^*_{2C}L$.

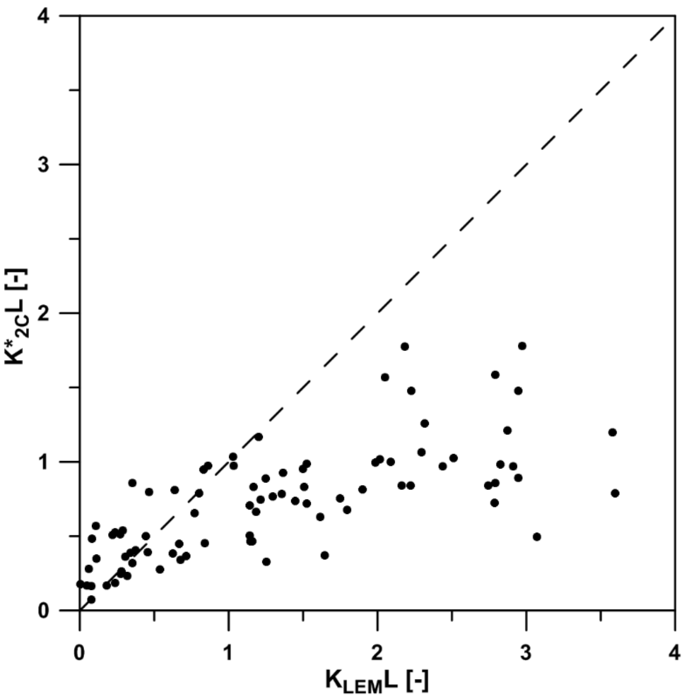

Figure 14 Comparison between experimental $K_{LEM}L$ and $K^*_{2C}L$.

A theoretical approach has been followed to better understand the behaviour of 2C technique. This analysis, which is described in Appendix 2, is based on dividing the flame profile in finite elements with defined k_{soot} and temperature. An accumulated radiated intensity is calculated for 650 and 550 nm and equation (3) is applied to obtain the corresponding $K_{2C}L$. At the same time, the optical thickness of the profile is calculated, which corresponds to $K_{LEM}L$. For different k_{soot} and temperature distributions (Figure 18), the corresponding $K^*_{2C}L$ and $K_{LEM}L$ have been obtained. Three data sets are presented in Figure 15. For each of them, the temperature profile and the value of Min K_{soot} were kept constant, while Max K_{soot} was modified to simulate the variation in the total soot mass within the flame. Values of Max K_{soot} have been varied between 45 (f_v = 13 ppm) and 370 (f_v = 50 ppm).

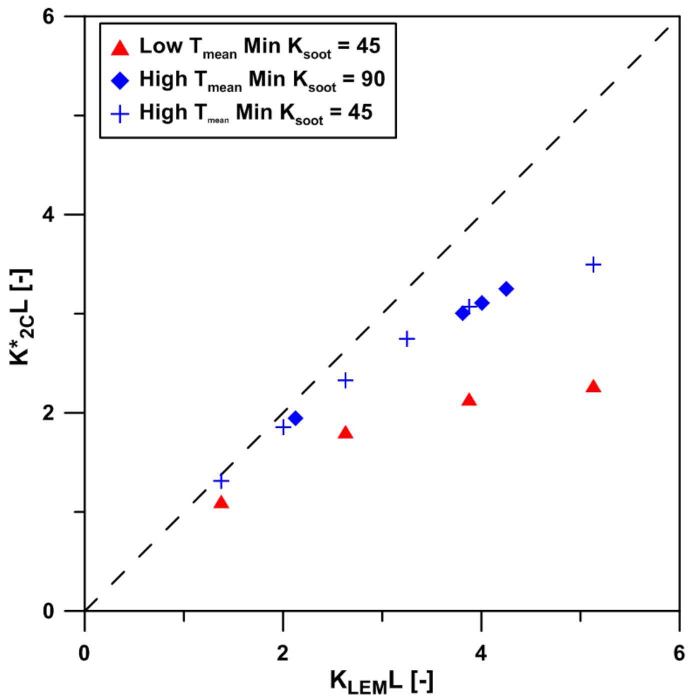

Figure 15 Theoretical comparison of $K_{LEM}L$ and $K_{2C}^{*}L$ for different k_{soot} and temperature distributions.

Theoretical calculations show a trend that is consistent with the experimental results presented in Figure 14. For the high T_{mean} case, no differences can be observed in $K_{2C}^{*}L$ when soot distribution shape is modified at constant $K_{LEM}L$. This suggests that the total amount of soot is more important than its distribution along the flame width. However, when the total soot amount changes ($K_{LEM}L$ increases) at constant T_{mean}, $K_{2C}^{*}L$ changes with a much lower sensitivity. This means that absorption effects within the optical path become relevant, and a fraction of the intensity emitted by the different soot layers does not reach the detectors. The difference between KL values from both techniques ranges from 20% for $K_{LEM}L \approx 1$ to almost 80% for $K_{LEM}L \approx 4$.

On the other hand, if both temperature profiles are compared at constant soot distribution, an increase in $K_{2C}^{*}L$ with T_{mean} is observed. This result agrees with recent measurements by Skeen et al. [39], where the ratio between KL as derived from LEM and spectral radiation measurements range from 1.5 at the highest temperature to 5 at the lowest temperature. Some explanation can be found by using the radiation propagation model. For that purpose, one has to keep in mind that the measured radiation is the result of the emitted radiation that propagates through the soot cloud and therefore becomes attenuated. The emission term depends on local temperature and soot amount, while the absorption one on the soot distribution. The measured radiation (and therefore temperature and KL factor) is therefore a weighted value along the line-of-sight. Derived results coincide with the real ones only if a uniform temperature distribution exists. If this is not the case, emitted radiation is biased towards the hottest part of the soot cloud, because of the non-linear temperature dependence of Planck's law. Considering the temperature variation in the previous plot, the high T_{mean} case has a more uniform temperature distribution, which results in a better agreement between $K^*_{2C}L$ and $K_{LEM}L$. When going to the low T_{mean} case, temperature gradients increase within the flame, and the influence of the outer (hotter) layers over the final measured radiation is more important than in the high T_{mean} case. This leads to larger differences between the soot as measured from the 2C and the real soot. Such effects decrease when soot concentration is low, as attenuation effects decrease and the contribution of the inner layers can still be maintained. Therefore, care must be taken when using results obtained from 2-Color Pyrometry under highly sooting conditions.

Similar arguments can be found in Musculus et al. [23] when comparing CFD calculations and experimental measurements of integrated radiation from the whole combustion chamber. These and other experimental references hint at the same conclusions, namely that 2C thermometry cannot resolve the full soot amount within the flame.

On the other hand, results in the previous section has shown that LII has a sensitivity to operating conditions and fuels comparable to LEM. However, some inconsistencies are present regarding the one-to-one comparison between LEM and LII, especially for the highest sooting operating condition, where a high discrepancy is found for hexadecane. It is known that LII can be strongly affected by phenomena like signal trapping or laser light attenuation [10], which would lead to a lack of LII signal at certain areas of the flame. This effect would be observable when $K_{LEM}L$ and S_{LII} were compared, as a deviation from linearity. De Francqueville et al. [13] have used this information to identify a set of experimental conditions where signal trapping is taking place, namely the situation where low LII signal is detected but high $K_{LEM}L$ is measured. In the present work, few cases show this behaviour (Figure 9). On the one hand, $K_{LEM}L$ was measured up to 60 mm from the nozzle orifice only for the reference points, while up to 50 mm for the rest of test conditions. Moreover, LII signal is triggered at a timing where the flame is in a quasi-steady state. Therefore, the high soot vortex is out of the field of view, and the high soot area is reached at mid-way through the observation window. In this sense, considering the distributions observed by the three techniques, the regions of maximum soot optical thickness were not measured with LEM.

Still, some cases exhibit the soot attenuation effects. Figure 16 shows the LII-derived soot volume fraction distribution from n-Decane (left) to n-Hexadecane (right) at P_c = 5.3 MPa, T_c = 900 K and P_{inj} = 100 MPa, corresponding to the evolution shown in Figure *12*. The general aspect of the 2D distribution is similar, with an increasing soot volume fraction with axial distance from the nozzle. When comparing fuels, n-Decane and 50Dec\50Hex show similarly low soot values. However, moving closer to pure n-Hexadecane results in higher soot. In particular, an apparent decrease of soot when moving from 30Dec to pure n-Hexadecane in regions downstream of 50 mm can only be explained in terms of strong attenuation processes within the flame. Moreover, in this region, soot distribution for n-Hexadecane becomes non-symmetrical, with higher values on the left side of the image. With the optical set up described previously, the laser sheet was entering from the left side of the flames shown in Figure 16. Thus, the previous effect could be interpreted as being due to either beam attenuation or signal trapping by soot particles, as it has been previously reported that both phenomena have a similar effect [11, 13].

The previous analysis invalidates the application of Equation (10) for the highest sooting condition due to strong signal trapping, which breaks the proportionality between LII signal and soot volume fraction. However, in the explored conditions, such effects are only present at some particular conditions, and the validity of LII as a semi-quantitative technique can be assumed as a fair argument.

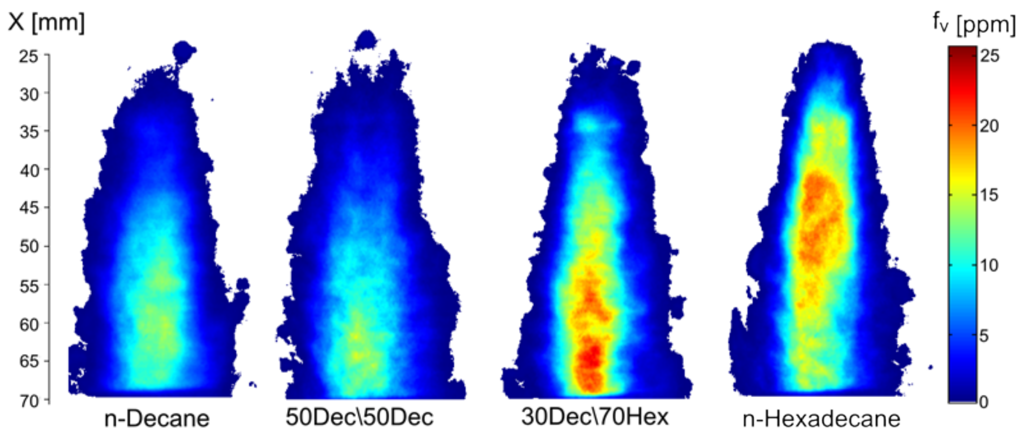

Figure 16 Soot volume fraction distribution for the four fuels at P_c = 5.3 MPa, T_c = 900 K and P_{inj} = 100 MPa.

5. CONCLUSIONS

Four different fuels were characterized in terms of soot formation. For this purpose, the three most extended optical techniques were used: Laser Extinction Method, 2-Color Pyrometry and Laser-Induced Incandescence. The three optical accesses available allowed applying the three techniques simultaneously, so that results were directly comparable. All the results have been analysed in order to determine the reliability and usefulness of each technique. The main conclusions are:

- In comparison with $K_{LEM}L$, $K_{2C}^{*}L$ presents in general lower values and its sensitivity to thermodynamic conditions and fuel properties is reduced. Moreover, it has been observed that $K_{2C}^{*}L$ seems to saturate when flame optical thickness increases. A further theoretical analysis suggested that the measurements are strongly influenced by soot and temperature distribution within the flame. When soot concentration is reduced ($K_{LEM}L \leq 1$), 2C is still reliable.
- Laser-Induced Incandescence makes it possible to measure the soot distribution at any plane within the flame, which is an advantage compared with line-of-sight diagnostics such as LEM and 2C. A calibration procedure based on the combination of LII signal and LEM measurements has been evaluated. The methodology has shown enough sensitivity to characterize the influence of the different experimental parameters. However, the beam attenuation and signal trapping effects have been observed to strongly influence on the measurements for the highest soot conditions and locations. Except for such cases, for most of the conditions LII can still be used as a semi-quantitative measurement technique.

LEM and LII have shown to be accurate enough to characterize the differences in soot formation for the four fuels considered in this study. It has been observed that the larger the molecule the more soot is formed. This results from a concurrent reduction in lift-off length, which implies lower oxygen entrainment at the flame base and therefore higher soot formation. A second important effect, though, is the inherent sooting tendency of the fuel type (TSI index), which increases with the molecule size for the investigated cases.

APPENDIX 1: Lift-off Length measurements

Visualization of OH*-Chemiluminescence at the base of the flame makes it possible to quantify the lift-off length (LoL). A gated 16-bit intensified CCD camera (Andor iStar) was utilized, equipped with a UV f/4 100 mm focal length lens. An interference filter centred at 310 nm (10 FWHM) was placed in front of the camera to remove the major part of the radiation of the flame while keeping OH*-Chemiluminescence. The camera was triggered at 6.6 after SoE while the intensifier was gated during 2.4 CAD and the gain was set to use the complete dynamic range of the camera without saturating it. Background segmentation was applied, based on a threshold value calculated as a percentage of the dynamic range of each image. This percentage was set to 10%, as it offered a good compromise for all the different test conditions. Then lift-off length was defined as the average distance between the nozzle and the ten nearest pixels of the flame.

In Figure A-1 LoL vs. fuel composition is presented, for different injection pressures (left) and in-cylinder pressures (right) f both in-cylinder temperatures. It can be observed that the LoL increases with the n-Decane fraction, which is consistent with the change in fuel reactivity (lower Centane number). LoL increases for all the fuels with injection pressure, while it decreases with in-cylinder pressure. However, differences are seen to decrease when in-cylinder pressure and temperature are increased. A similar effect is observed when the injection pressure is decreased.

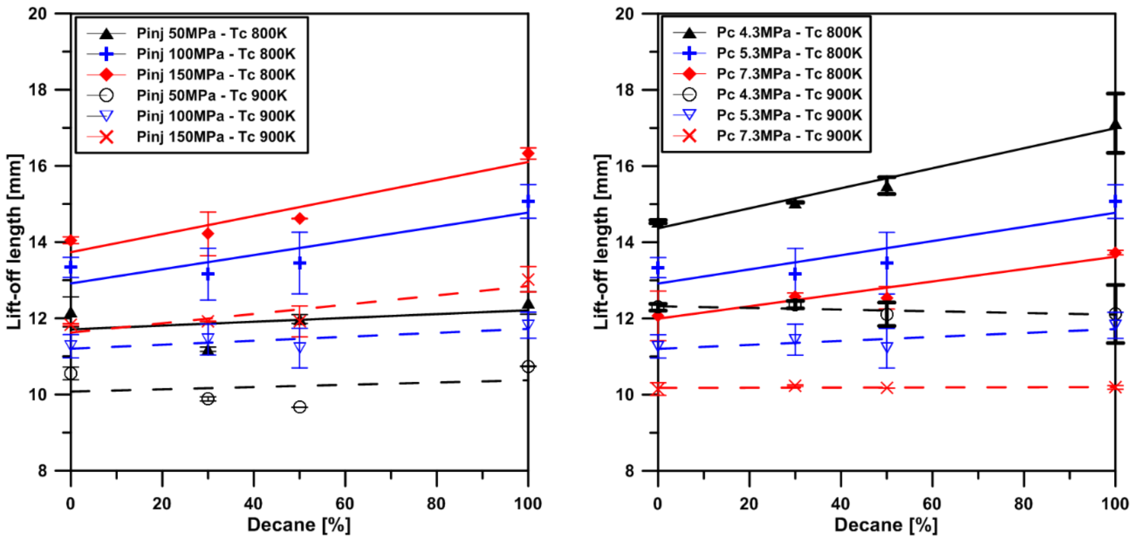

Figure 17 Lift-off length vs. n-Decane content, for different injection pressures (left) and different in-cylinder pressures (right), at 800 and 900 K in-cylinder temperature.

APPENDIX 2 – Radiation propagation model

Simple radiation propagation concepts have been used to improve the understanding of the differences between $K_{2C}L$ and $K_{LEM}L$, following a similar methodology as Payri et al. [22]. These authors described the behaviour of the 2-Colour Pyrometry technique under different in-cylinder conditions and compared experimental measurements with theoretical predictions, based on the equations shown in the previous sections.

A flame profile, perpendicular to its axis, can be discretized as an axisymmetric distribution of layers, with constant k_{soot} and temperature. Each of this layers both emits ($I_{soot,i}$) and absorbs (α_i) radiation from the previous layers. Thus, the intensity measured by one detector on one side of the flame is the result of an accumulation of emission and absorption processes along the optical path, through all the layers inside the flame. $I_{soot,i}$ is calculated by equation (3) while α_i is obtained from equation (5). Finally, it is possible to calculate the corresponding optical thickness of the profile ($K_{LEM}L$) as the accumulation of the $K_{LEM}L_{,i}$ from the different "i" layers inside the flame as it is defined by equation (12).

$$K_{LEM}L = \sum_{i=1}^{2R} 2.519 k_{soot,i} L_i \quad (12)$$

Where R represents the maximum radius of the profile and L is the width of each layer. Several flame temperature and k_{soot} radial distributions have been evaluated, based on previously published experimental results [22], which are shown in Figure 18. It must be noted that this approach assumes instantaneous oxidation of soot at the diffusion flame front. Therefore, radial distribution of both Temperature and k_{soot} are only considered until that particular location. The shape of k_{soot} profile was kept constant for all the calculations while the Min k_{soot} and Max k_{soot} were modified to vary the total amount of soot. The temperature profile shape was kept also constant, but the minimum value was modified in order to evaluate its influence on the final measured $K_{2C}L$. Peak temperature was fixed at 2800 K, close to the values obtained at the edge of the flame for T_c = 900 K cases.

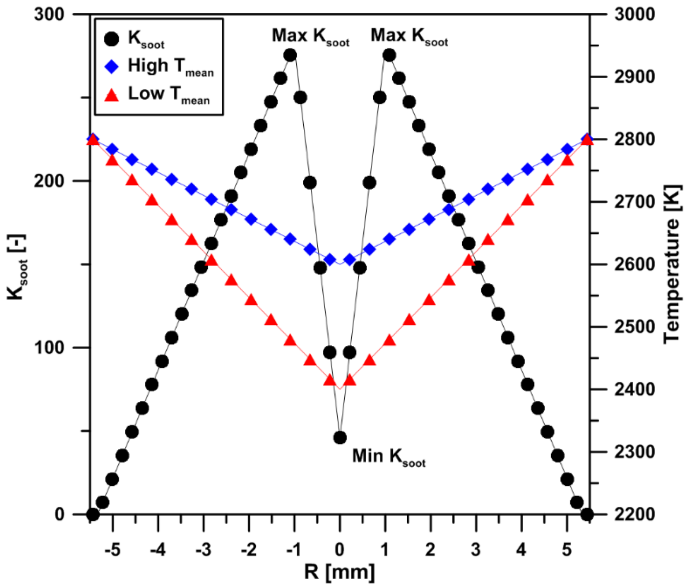

Figure 18 Theoretical radial profiles for k_{soot} and flame temperature distribution

Acknowledgments

Authors wold like to acknowledge that part of this work has been funded by the Spanish Ministry of Science and Technology through project TRA2011-26359 and grant BES-2012-059721. Some other parts of this works was financially supported by "COMET K2 - Competence Centres for Excellent Technologies Programme" (project B03T02). In addition, the authors acknowledge that some equipment used in this work has been partially supported by FEDER project funds (FEDER-ICTS-2012-06)", framed in the operational program of unique scientific and technical infrastructure of the Ministry of Science and Innovation of Spain.

References

[1] I. M. Kennedy, *Progress in Energy and Combustion Science,* vol. 23, no. 2, pp. 95 - 132, 1997.

[2] D. R. Tree and K. I. Svensson, *Progress in energy and combustion science,* vol. 33, pp. 272-309, 2006.

[3] M. P. B. Musculus, *SAE Technical Papers,* 2006, doi: 10.4271/2006-01-0079

[4] M. K. Bobba and M. P. B. Musculus, *Combustion and Flame,* vol. 159, no. 2, pp. 832-843, 2012.

[5] J. E. Dec, *SAE Technical paper series,* 1992, doi: 10.4271/920115

[6] L. M. Pickett and D. L. Siebers, *SAE Technical Papers,* 2003, doi: 10.4271/2003-01-3080

[7] T. Ito, T. Hosaka, M. Ueda, J. Senda and H. Fujimoto, *SAE Technical Papers,* 2004, doi: 10.4271/2004-01-1398

[8] K. Lee, Y. Han, W. Lee, J. Chung and C. Lee, *Measurement Science and Technology,* vol. 16, no. 2, pp. 519-528, 2005.

[9] X. He, X. Ma and J. Wang, *Ranshao Kexue Yu Jishu/Journal of Combustion Science and Technology,* vol. 15, no. 4, pp. 344-349, 2009.

[10] C. Schulz, B. F. Kock, M. Hofmann, H. Michelsen, S. Will, B. Bougie, R. Suntz and G. Smallwood, *Applied Physics B: Lasers and Optics,* vol. 83, no. 3, pp. 333-354, 2006.

[11] J. V. Pastor, J. M. García, J. M. Pastor and J. E. Buitrago, *Measurement Science and Technology,* vol. 17, no. 12, pp. 3279-3288, 2006.

[12] S. Kook and L. M. Pickett, *Proceedings of the Combustion Institute,* vol. 33, no. 2, pp. 2911 - 2918, 2011.

[13] L. de Francqueville, G. Bruneaux and B. Thirouard, *SAE Int. J. Engines 3,* vol. 1, pp. 163-182, 2010.

[14] T. Henriksen, G. Nathan, Z. Alwahabi, N. Qamar, T. Ring and E. Eddings, *Combustion and Flame,* vol. 156, no. 7, pp. 1480-1492, 2009.

[15] S. Kook and L. M. Pickett, *SAE Technical Papers,* 2009, doi: 10.4271/2009-01-2643

[16] E. Cenker, G. Bruneaux, L. M. Pickett and C. Schulz, *SAE International Journal of Engines,* vol. 6, no. 1, pp. 352-365, 2013.

[17] J. Yan and G. L. Borman, *SAE Technical Papers,* 1988, doi: 10.4271/881315

[18] H. X. Quoc, J.-M. Vignon and M. Brun, *SAE Technical Papers,* 1991, doi: 10.4271/910736

[19] H. Zhao and N. Ladommatos, *Progress in Energy and Combustion Science,* vol. 24, no. 3, pp. 221-255, 1998.

[20] J. Vattulainen, V. Nummela, R. Hernberg and J. Kytölä, *Measurement Science and Technology,* vol. 11, no. 2, pp. 103-119, 2000.

[21] K. I. Svensson, A. J. MacKrory, M. J. Richards and D. R. Tree, *SAE Technical Paper,* 2005, doi: 10.4271/2005-01-0648.

[22] F. Payri, J. V. Pastor, J. M. García and J. M. Pastor, *Measurement Science and Technology,* vol. 18, no. 8, pp. 2579-2598, 2007.

[23] M. P. Musculus, S. Singh and R. D. Reitz, *Combustion and Flame,* vol. 153, pp. 216-227, 2008.

[24] J.-G. Nerva, An Assessment of fuel physical and chemical properties on the combustion of a Diesel spray, Universitat Politècnica de València, Departamento de Máquinas y Motores Térmicos, 2013.

[25] A. Diez, H. Zhao, T. Carrozzo, A. E. Catania and E. Spessa, *Proceedings of the Institution of Mechanical Engineers, Part D: Journal of Automobile Engineering,* vol. 226, no. 5, pp. 684-697, 2012.

[26] J. Zhang, W. Jing, W. Roberts and T. Fang, *Applied Energy,* vol. 107, pp. 52-65, 2013.

[27] W. Jing, W. Roberts and T. Fang, *SAE Technical Papers,* 2014, doi: 10.4271/2014-01-1251

[28] M. P. Musculus, J. E. Dec and D. R. Tree, *SAE Technical Papers,* 2002, doi: 10.4271/2002-01-0889

[29] L. M. Pickett and D. L. Siebers, *Combustion and Flame,* vol. 138, pp. 114-135, 2004.

[30] M. P. Musculus and L. M. Pickett, *Combustion and Flame,* vol. 141, no. 4, pp. 371-391, 2005.

[31] F. Payri, J. V. Pastor, J.-G. Nerva and J. M. García-Oliver, *SAE International Journal of Engines,* vol. 4, no. 2, pp. 2278-2297, 2011.

[32] J. Manin, L. M. Pickett and S. A. Skeen, *SAE International Journal of Engines,* vol. 6, no. 4, 2013.

[33] V. Bermúdez, J.M. García, E. Juliá and S. Martínez, *SAE Technical Papers,* 2003, doi: 10.4271/2003-01-1110

[34] H. C. Hottel and F. P. Broughton, *Industrial and Engineering Chemistry,* vol. 4, no. 2, pp. 166-175, 1932.

[35] K. I. Svensson, A. J. MacKrory, M. J. Richards, and D. R. Tree, *SAE Technical Papers,* 2005, doi: 10.4271/2005-01-0648

[36] L. Pickett, D. Siebers and C. Idicheria, *SAE Paper,* 2005, doi: 10.4271/2005-01-3843

[37] A. Mensch, R. Santoro, T. Litzinger and S.-Y. Lee, *Combustion and Flame,* vol. 157, no. 6, pp. 1097 - 1105, 2010.

[38] K. I. Svensson, "Effects of fuel molecular structure and composition on soot formation in direct-injection spray flames," *Brigham Young University, Department of Mechanical Engineering,* 2005.

[39] S. Skeen, J. Manin, L. M. Pickett, K. Dalen and A. Ivarsson, *SAE Technical Paper,* 2014, doi: 10.4271/2014-01-1252